## Werk

**Jahr:** 1982
**Kollektion:** fid.geo
**Signatur:** 8 Z NAT 2148:51
**Digitalisiert:** Niedersächsische Staats- und Universitätsbibliothek Göttingen
**Werk Id:** PPN1015067948_0051
**PURL:** http://resolver.sub.uni-goettingen.de/purl?PPN1015067948_0051

**LOG Id:** LOG_0020
**LOG Titel:** Comparative interpretation of explosion seismic data
**LOG Typ:** article

## Übergeordnetes Werk

**Werk Id:** PPN1015067948
**PURL:** http://resolver.sub.uni-goettingen.de/purl?PPN1015067948
**OPAC:** http://opac.sub.uni-goettingen.de/DB=1/PPN?PPN=1015067948



## Contact

Niedersächsische Staats- und Universitätsbibliothek Göttingen
Georg-August-Universität Göttingen
Platz der Göttinger Sieben 1
37073 Göttingen
Germany
Email: gdz@sub.uni-goettingen.de

J Geophys (1982) 51:69–84

Journal of Geophysics

# Comparative Interpretation of Explosion Seismic Data

J. Ansorge[1], C. Prodehl[2], and D. Bamford[3],
with contributions by: E. Banda[1], E.N. Bessonova[4], L.W. Braile[5], V.M. Fishman[4], E. Flüh[6], V.S. Geyko[4], P. Giese[7], D.P. Hill[8], J.G. Jurov[4], I.P. Kosminskaya[4], W.D. Mooney[8], G. Müller[9], St. Mueller[1], S. Mykkeltveit[10], J.A. Orcutt[11], N.I. Pavlenkova[4], E.L. Reznikov[4], G.A. Sitnikova[4], and R.B. Whitmarsh[12]

[1] Institute of Geophysics, ETH-Hönggerberg, CH-8093 Zürich, Switzerland
[2] Geophysikalisches Institut, Hertzstr. 16, D-7500 Karlsruhe 21, Federal Republic of Germany
[3] British Petroleum Company, Geophysics Research Division, Britannic House, Moor Lane, London, England
[4] Institute of Physics of the Earth, B. Gruzinskaya 10, Moscow, B-242, USSR
[5] Department of Geosciences, Purdue University, West Lafayette, IN 47907, USA
[6] Geophysikalisches Institut, Olshausenstr. 40–60, D-2300 Kiel, Federal Republic of Germany
[7] Institut für Geophysikalische Wissenschaften, FU, Rheinbabenallee 49, D-1000 Berlin 33
[8] U.S. Geological Survey, 345 Middlefield Road, Menlo Park, CA 94025, USA
[9] Universitätsinstitut für Meteorologie und Geophysik, Feldbergstr. 47, D-6000 Frankfurt a. Main 97, Federal Republic of Germany
[10] NTNF/NORSAR, P.O. Box 51, N-2007 Kjeller, Norway
[11] Scripps Institute of Oceanography, La Jolla, CA 92093, USA
[12] Institute of Oceanographic Sciences, Wormley, Godalming, Surrey GU8 5UB, England

**Abstract.** A workshop of the Commission on Controlled Source Seismology in the International Association of Seismology and Physics of the Earth's Interior was held at Karlsruhe, F.R.G., on August 1–6, 1977. The aim was the comparison of various interpretations derived from a set of several explosion seismic data. These same data had been distributed to the participants before the meeting who interpreted them by different inversion methods. In the workshop itself the interpretations of the various authors were discussed, especially with respect to differing or conflicting results. Out of the distributed data two sets were discussed in more detail: A synthetic crustal record section whose source structure was not known to the participants, and a record section of real field data which was part of the LISPB experiment through the British Isles in 1974. Methods of interpretation were based on the travel-time information and the calculation of synthetic seismograms. This paper summarizes and compares the interpretations achieved before, during and after the workshop. The variety of velocity-depth functions reflects primarily the differences in the correlation of phases by the various workers. Nevertheless, it can be concluded that the main structural characteristics for both data sets were worked out by all participants.

The use of synthetic seismograms during the interpretation of seismic data proved to be very important in arriving at a model which approximates the truth from among the many possible velocity-depth models which satisfy the travel-time observations alone. Only laterally homogeneous structures were considered in this workshop.

Institute of Geophysics, Zürich, Contribution No. 360
Geophysical Institute, Karlsruhe, Contribution No. 247

**Key words:** Crustal structure – Explosion seismic data – Interpretation methods – Travel times – Synthetic seismograms

## Introduction

The Commission on Controlled Source Seismology (CCSS) in the International Association of Seismology and Physics of the Earth's Interior (IASPEI) held a workshop on "Comparative Interpretation of Explosion Seismic Data" at Karlsruhe, West Germany, on August 1–6, 1977. A prime objective of this workshop was for a group of seismologists to compare independent interpretations of a number of identical data sets provided before the meeting in the form of record sections. The groups were free to use whatever inversion methods they preferred.

Two out of five data sets of different character and origin which received the highest attention will be discussed here in detail: A synthetic record section for a crustal structure which was kept unknown to the interpreters (Data Set 1), and a crustal record section from the LISPB experiment in Great Britain (Data Set 2) (Bamford et al., 1976; 1978). Both data sets contained only compressional phases. To stimulate fruitful discussions, participants were requested to submit their interpretations well in advance in order to distribute them prior to the workshop. Thirty participants contributed to the workshop, and those listed as authors have been working intensively with the two data sets discussed here.

The success of the workshop was greatly enhanced by the direct access to computer facilities which allowed the

0340-062X/82/0051/0069/$03.20

immediate computations of travel times and synthetic seismograms for models as they resulted during the discussions. A summary of the results was presented at a poster session of the IASPEI meeting in 1977 in Durham, England (Bamford et al., 1979).

### Data Set 1: Synthetic Record Section

The inversion of a synthetic record section computed for a given crustal model has the advantage that it is possible to check how closely the inverted models approximate the given "true" model. Furthermore any discrepancies in correlation or identification of secondary arrivals and how much they affected the inversion could be studied, since the phase-identifications in terms of the original model were available during the workshop.

Figure 1 shows a simple crustal model from which the synthetic record section in Fig. 2 was computed in Karlsruhe, using the reflectivity method (Fuchs and Müller, 1971). In order to produce a realistic case numerical noise was added to the synthetic seismograms. The resulting interferences caused phases which could be mistaken as true arrivals due to structure, as will be seen in the following discussions. Twelve different velocity-depth models were produced by participants of the workshop (Fig. 3).

Out of the many methods of interpretation for crustal refraction data only the most frequently used were applied to these data and only those will be discussed in detail.

Models B, C, D, F, G and H come very close to the original structure A and vary little from each other. The models B, C, D, F were derived using the following scheme:

– Prograde travel-time branches were correlated and a preliminary model from apparent velocities and intercept times was determined. Critital distances were fixed by the qualitative study of amplitudes.

– Travel-time curves by stepwise adjustment were calculated, starting from the previously derived preliminary model.

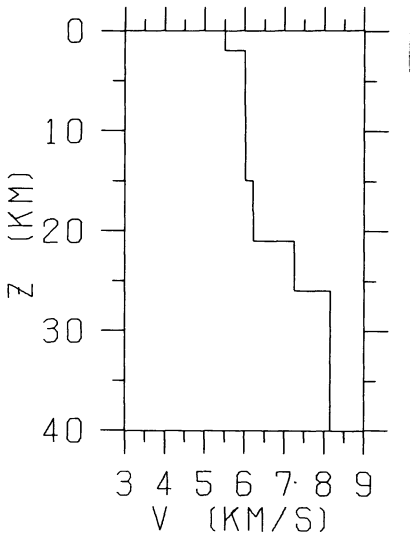


**Fig. 1.** Model for the synthetic record section (Data Set 1) in Fig. 2

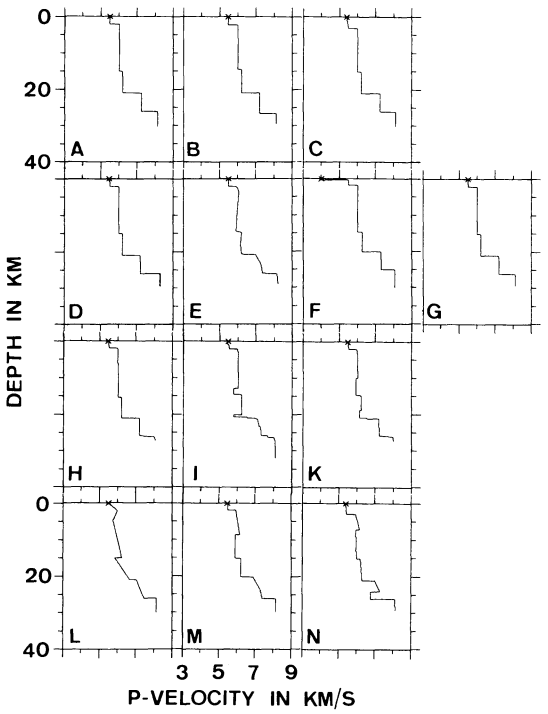


**Fig. 3.** Models derived from the synthetic record section in Fig. 2 by various authors: *A*) Original model; *B*) G. Müller; *C*) Braile; *D*) Ansorge, St. Mueller, Banda; *E*) Giese; *F*) Flüh; *G*) Mykkeltveit; *H–K*) Bessonova, Fishman, Reznikov, Sitnikova; *L*) Geyko; *M*) Jurov; *N*) Pavlenkova

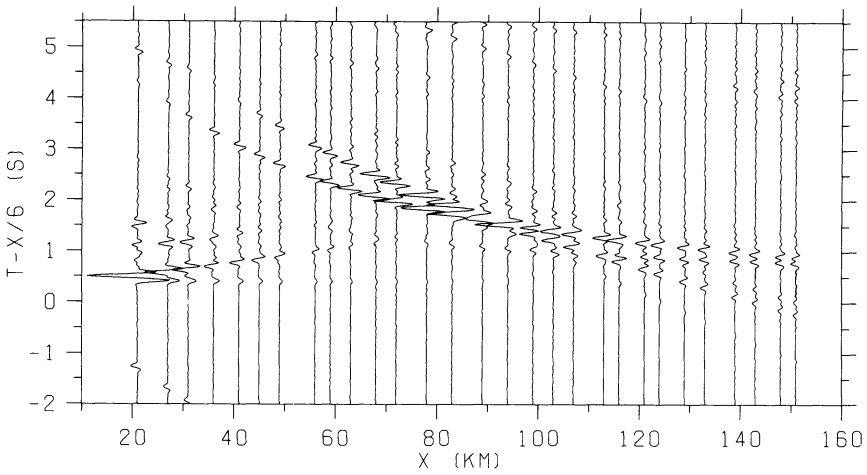


**Fig. 2.** Synthetic crustal record section with true amplitudes (Data Set 1) distributed prior to the workshop (Reduction velocity = 6 km/s, $v_P/v_S = \sqrt{3}$, $\rho = 0.252 + 0.3788 \cdot v_P$)

– Synthetic seismograms were calculated by means of ray theoretical methods (Červený et al., 1977) or the reflectivity method by Fuchs and Müller (1971).

Figure 4 shows an example of travel-time curves for model D (Fig. 3). Synthetic seismogram sections are shown in Figs. 5 and 6 for models D and F (Fig. 3), using the ray theoretical and reflectivity methods, respectively. In all cases the travel times and amplitudes fit the original data quite well. Models B, D and F contain no velocitiy gradients, in agreement with the original model.

Mykkeltveit (Model G, Fig. 3) uses a different approach (Mykkeltveit, 1980). After identifying one arrival as the reflection from an interface, he varies the angle of incidence and calculates for each ray pairs of velocity $v$ and depth $z$, which lead to the same value of travel time $t$ and distance $x$ thus forming a curve in the $v,z$-diagram. This procedure is repeated for another arrival of the same phase, i.e. the same reflection observed at a different distance. The intersection of the corresponding two curves in the $v,z$-diagram defines the correct velocity-depth value for this reflection. This method is applied after the parameters of the top layers have been deduced by conventional means from the correlations $c$ and $b$ in Fig. 7. The arrows of Fig. 7 show the choice of points for modelling the structure at greater depths. Once a layer is identified, it is included in the known velocity distribution and the procedure is repeated for the determination of $v$ and $z$ in the next layer. Finally, the velocity of the lower halfspace is estimated from the apparent velocity of the refracted wave $h$ in Fig. 7. The resulting velocity-depth model G in Fig. 3 is almost identical to the original one. This excellent agreement is obtained thanks to the existence of very well developed under- and over-critical reflections, due to the first-order discontinuities.

Another inversion technique is applied by Giese (Fig. 8). Starting with a very similar correlation of travel-time curves (see for comparison Figs. 4 and 8), he determines a first approximate model using, for prograde branches, the equation

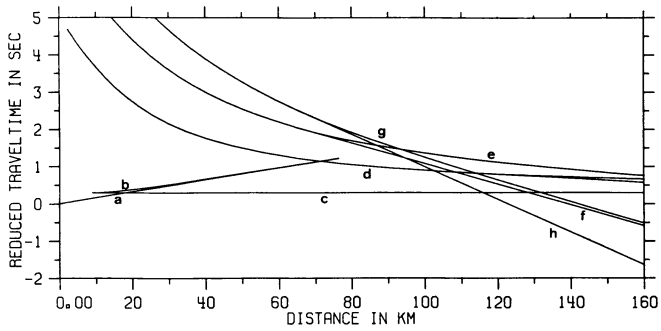


**Fig. 4.** Travel-time curves by Ansorge, Mueller, Banda for Data Set 1 (Fig. 2), (reduction velocity 6 km/s)

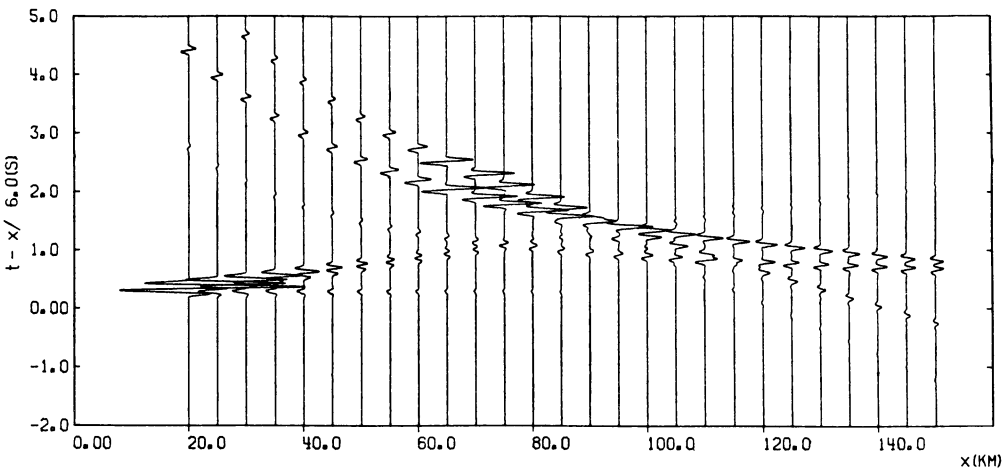


**Fig. 5.** Synthetic record section by Ansorge, Mueller, Banda calculated for Data Set 1 using the ray theoretical method (Červený et al., 1977)

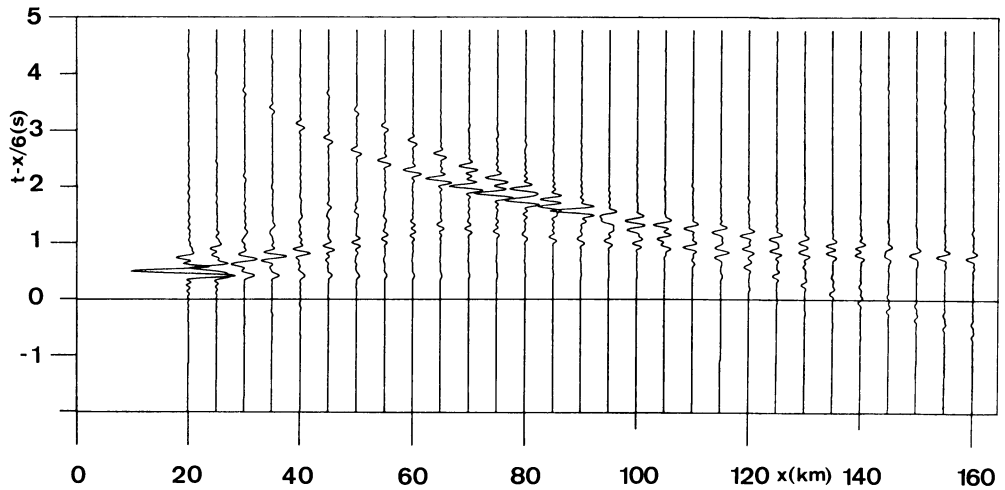


**Fig. 6.** Synthetic record section by Flüh for Data Set 1 using the reflectivity method (Fuchs and Müller, 1971)

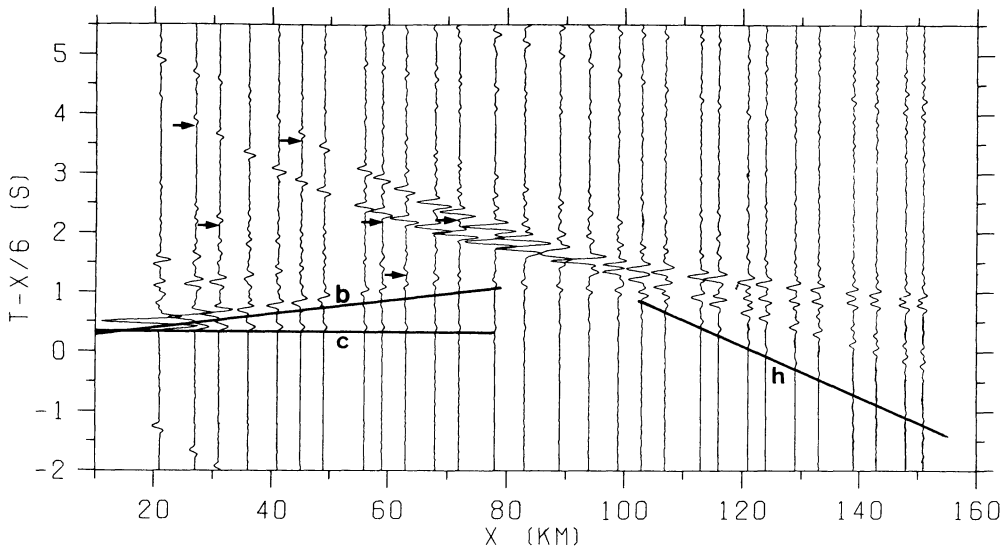


**Fig. 7.** Correlations of travel times in Data Set 1 by Mykkeltveit

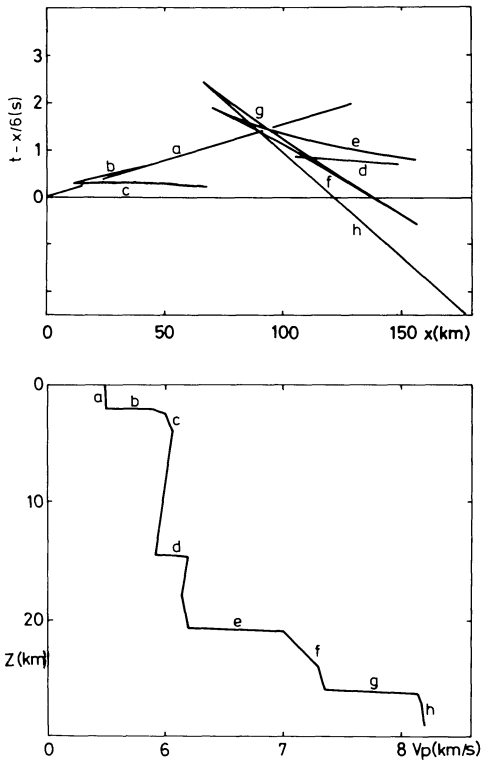


**Fig. 8.** Travel-time curves and model E (Fig. 3) for Data Set 1 by Giese

$$z_P = \frac{x}{2} \cdot \sqrt{\frac{v_P \cdot t/x - 1}{v_P \cdot t/x + 1}} \quad \text{with } v_P = dx/dt,$$

and for retrograde branches the equation

$$z_{\max} = \frac{x}{2} \cdot \sqrt{v_P \cdot t/x - 1},$$

as well as the $x^2 - t^2$ method (Giese, 1976).

This first model already contains velocity gradients. Negative velocity gradients are then introduced in order to limit the observed distance of certain travel-time branches, e.g. phase *c* in Fig. 8. The resulting model (Fig. 8 and model E in Fig. 3) deviates slightly from the original one, but the main structural features are clearly obtained. This model was not specially checked, however, by the recalculation of synthetic seismograms.

The models H to N in Fig. 3 have been determined by methods widely used in the USSR. The interpretations were based only on the kinematic features of the waves. Starting with essentially the same correlation as shown in Fig. 9, the travel-time branches are identified as reflected or refracted phases in a first step for all models.

Bessonova, Fishman, Reznikov and Sitnikova used the so-called Tau-method (Bessonova et al., 1974, 1976) to derive models H to K in Fig. 3. After correlating travel-time curves in the record section, discrete travel times $t(x)$ are inverted into delay times $\tau(p) = t(p) - px(p)$, $p$ being the ray parameter. Bounds on the delay times arising from a given accuracy of travel times $t(x)$ are used to generate extreme bounds on the velocity-depth distribution (Fig. 10), which themselves are not possible solutions.

Based on the correlations chosen by Bessonova et al. with an accuracy of $\pm 0.03$ s, the deduced extremal bounds on the velocity-depth distribution (Fig. 10) do not exclude the possibility of low-velocity zones. Consequently the two models I and K in Fig. 3, which are those preferred by the authors from the variety of possible models, show details which the original model does not contain. Models H to K satisfy the travel-time observations equally well. Phases caused by the upper boundaries of low-velocity zones may easily be missed depending on the actual signal to noise ratio. In addition, the relative amplitudes of phases are widely governed by the velocity gradients across boundary zones; therefore only the use of synthetic seismograms allows separation of models with the same kinematic character. Model L (Fig. 3) was determined using a program by Geyko (1970), which is based on the method developed by Gerver and Markushevich (1967). In this procedure the depths of reflectors are estimated from the near-critical reflections and the vertical velocity gradient above the reflectors from the reversed branches. The entire time-distance curves are used for the determination of minimum and maximum velocity in the layer between the reflectors. Thus the solution for each layer, i.e. for each segment of the function

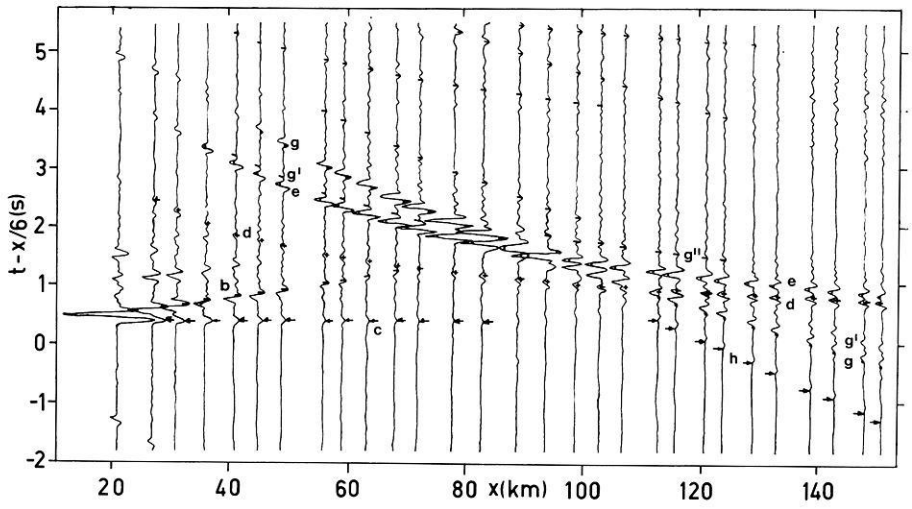


**Fig. 9.** Data Set 1 with travel-time correlations by Jurov and Pavlenkova

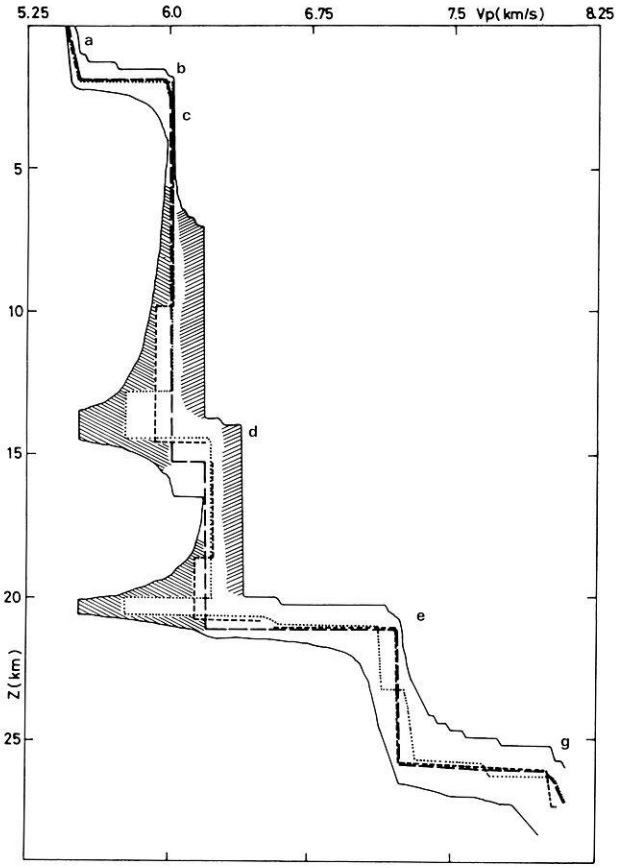


**Fig. 10.** Velocity-depth structure for Data Set 1 by Bessonova et al. — boundaries of the region of all possible structures (Tau-method); velocity-depth models with: .....wide-low-velocity zone (Model I in Fig. 3); -----narrow low-velocity zone (Model K in Fig. 3); – – – – without low-velocity zone (Model H in Fig. 3)

$v(z)$, consists of three parameters: the lower boundary of the layer, the maximum velocity and the minimum velocity in the layer. The depths of $v_{\min}$ and $v_{\max}$ depend on the velocity gradient obtained (Model L, Fig. 3). This model agrees with the observed travel times to within the standard deviation of $\pm 0.05$ s, although the resulting amplitudes have not been checked.

Model M (Fig. 3) was derived by Jurov who identified the nature of the phases *b, d, e, g* (Fig. 9) either as refracted or reflected arrivals by the analysis of the effective velocity, $v_e(x)$ (Riznichenko, 1946):

$$v_e(x) = \sqrt{\frac{x}{t} \cdot \frac{dx}{dt}}.$$

If $v_e(x)$ is constant or increases with $x$, the wave is considered to be a reflection, if $v_e(x)$ decreases with $x$, the wave is considered to be a refraction or diving wave. Velocity depth functions were calculated by assuming first-order discontinuities, which allows the $t^2 - x^2$ method for reflections (Fig. 11) and the intercept-time method for refractions. Jurov (1978) concludes that the vertical average velocity $\bar{v}$ is related to the effective velocity $v_e$ at $x/2z \cong 0.5$–$2.0$ by $\bar{v} \cong 0.995\ v_e$ for reflections from boundaries in the upper crust and $\bar{v} \cong 0.98\ v_e$ for $P_M P$ reflections.

The $\bar{v}$-values were used for the calculation of layer velocities. These were compared with the apparent velocities of the waves *b, d, e, g* (Fig. 9) at large distances. Slight differences were observed only for the layer between the boundaries *b* and *d*. Its layer velocity was determined as 5.985 km/s while the apparent velocity of the wave *c* at the distance range 50–70 km is 6.01 km/s. It was supposed, therefore, that two layers exist between the boundaries *b* and *d*. In the upper layer the velocity increases with depth up to 6.01 km/s, in the second layer the velocity is smaller. To prove this assumption an attempt was made to identify reflections from the top of the low-velocity layer. Such reflections were not found, but it is possible to consider the wave *g''* as peg-leg reflections (a channel wave) inside the low-velocity layer (Fig. 9). The next layer considered in detail was the fifth layer having a gradient zone at a depth 21–24 km in model M (Fig. 3), which corresponds to the time-distance curve *g* (Fig. 9). This zone is caused by a correlation where $v_e(x)$ seems to decrease with $x$ because of interference between phases *e* and *g* (Fig. 9). The $t(x)$ curves calculated for the model M of Fig. 3 coincide with the correlated curves within a standard deviation of $\pm 0.03$ s.

Pavlenkova (Model N, Fig. 3) inverts the first-arrival times into depth using a formula by Pavlenkova and Smeljanskaja (1969):

$$z = \frac{x}{2} \sqrt{\frac{v_P - \bar{v}}{v_P + \bar{v}}};$$

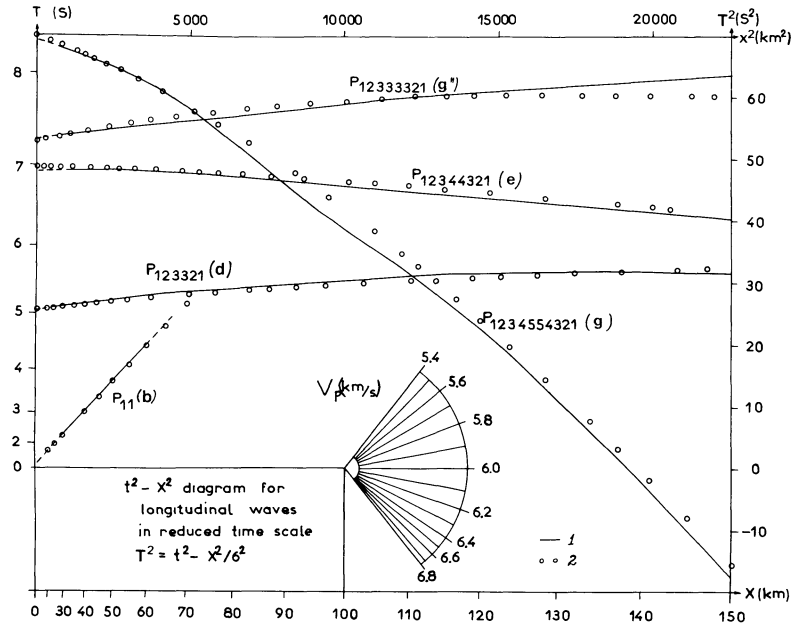


**Fig. 11.** $t^2-x^2$ diagram for Data Set 1 in reduced time scale by Jurov, *1* travel-time curves taken from Fig. 9 and used for the calculation of Model M in Fig. 3; *2* travel times calculated from true model (Fig. 1)

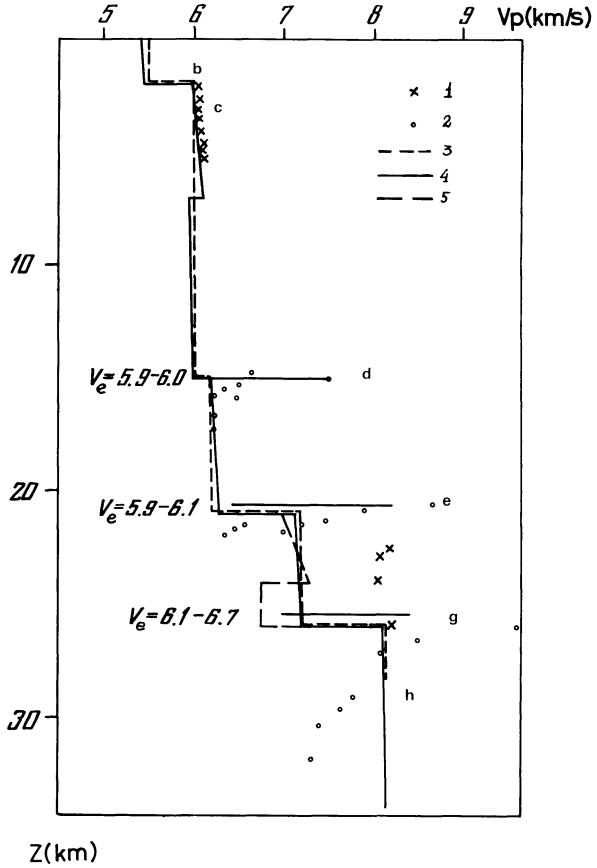


**Fig. 12.** Model by Pavlenkova *1* Values obtained from first arrivals *2* Values obtained from reflections with different effective velocities $v_e(x)$ *3* True model (Fig. 1) *4* Model N with simplified lower crust *5* Model N (Fig. 3)

where $\bar{v}=\frac{x}{t}$ and $v_P$ is the apparent velocity at distance $x$. The obtained depths $z(v_P)$ are plotted as crosses in Fig. 12. Pavlenkova assumes that the average velocity $\bar{v}$ is equal to the effective velocity $v_e(x=0)$, therefore, for the reflections *b, d, e, g* (Fig. 9) the average velocities $\bar{v}=v_e(x)$ or $v_e(v_P)$ and depths $z(v_e)$ or $z(v_P)$ are determined point by point. The depths are plotted versus $v_P$ as open circles in Fig. 12. To determine the real depth of the boundary it is necessary to take $z$ from the curve $z(v_P)$ at the largest $v_P$ which corresponds to the time-distance curve minimum in reduced scale. The lowest $v_P$ of a reflection determines the highest layer velocity in the medium above the reflector. Thus, three main values were estimated for each reflection: The depth of the interface, the maximum layer velocity ($v_P$) above it and the average velocity. Between the boundaries *d, e, g* (Fig. 12) maximum-layer velocities of 6.25 and 7.15 km/s were deduced. For the upper part between interfaces *b* and *d* the apparent velocity of first arrivals increases from 6.0 to 6.1 km/s. However, for the entire layer an average velocity of 6.0 km/s was determined. A low-velocity layer, therefore, had to be introduced (Fig. 12). After checking the model by the calculation of travel times, only slight depth corrections of the reflectors were necessary (continuous line in Fig. 12). Considerable deviations in the depth to the Moho appear between the determinations from reflections and refracted arrivals (see crosses in lower part of Fig. 12). In order to explain the weak phases $g'$ (Fig. 9) a low-velocity layer was assumed immediately above the Moho.

The three models L, M, N in Fig. 3 are in good agreement with the given time-distance curves. Depths of the main discontinuities and average velocities based on the strong reflections have values similar to those in the initial model, irrespective of the method with which these values were derived. In comparison with the original model, depths differ by not more than 200 m and average layer velocities by not more than 0.05 km/s.

All three models have, however, similar additional details. Low-velocity layers are caused by the correlation of first or later arrivals with too high apparent velocities. This leads to positive velocity gradients in the top layer which are not real. Furthermore, the introduction of low-velocity layers is supported by the correlation of weak phases $g'$ and $g''$ (Fig. 9) which have been interpreted as

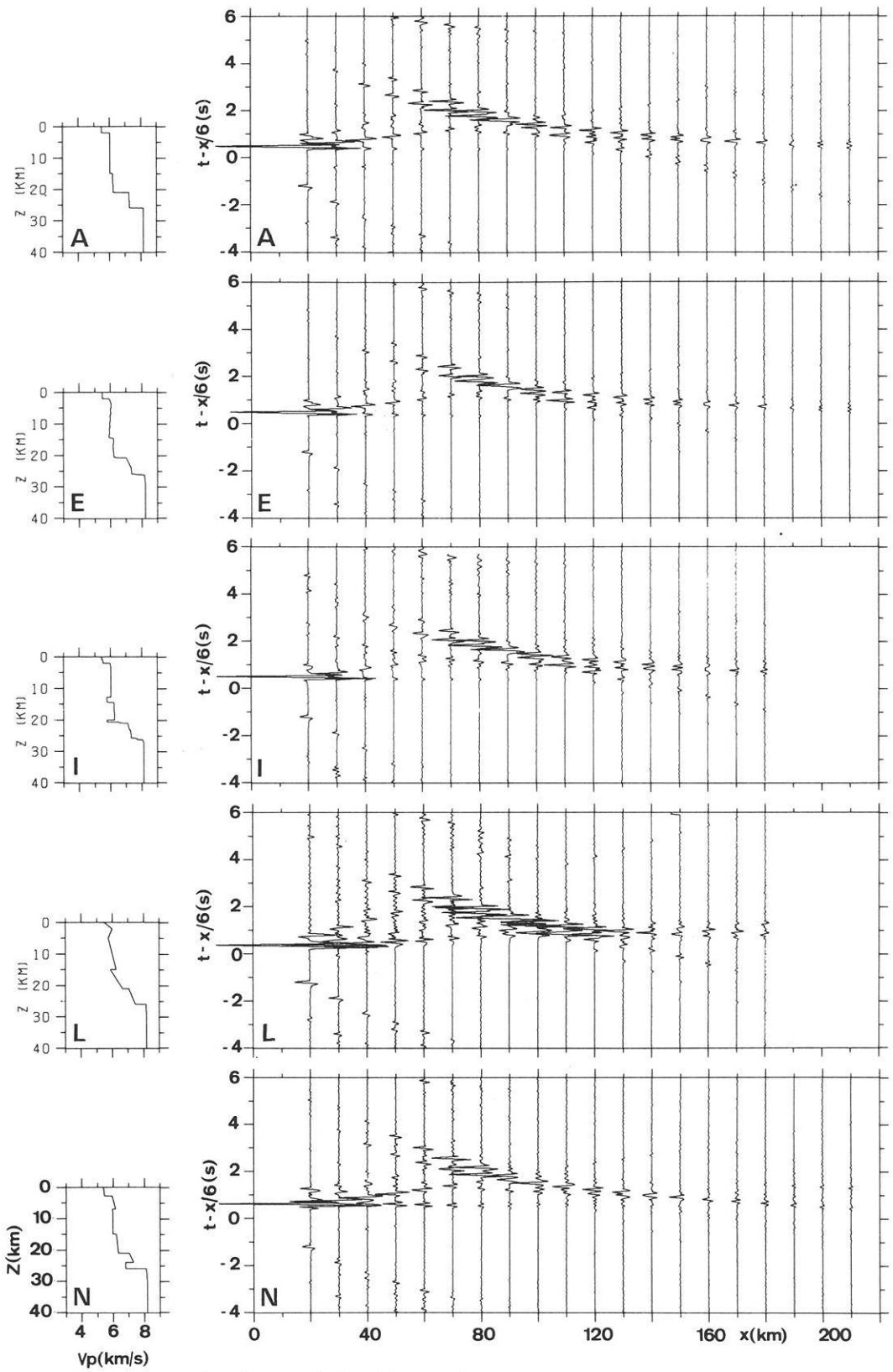


**Fig. 13.** Synthetic record sections recalculated from various models for Data Set 1 (reduction velocity 6 km/s)

multiple reflections inside such layers. From later calculations of time-distance curves for the initial model, Jurov concludes that these phases $g'$ and $g''$ may also be interpreted as converted waves.

During the workshop synthetic record sections (Fig. 13) were calculated for some representative velocity-depth models from Fig. 3 (Models E, I, L, N), which deviate substantially from the original model. For better comparison, a

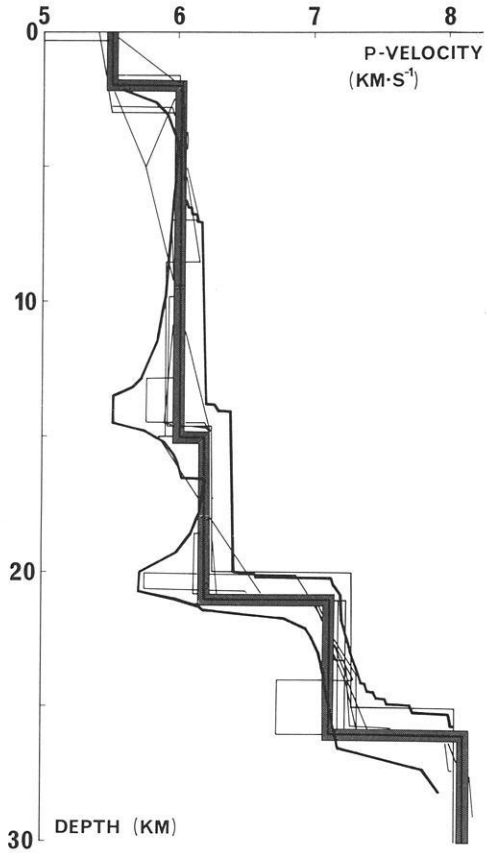


**Fig. 14.** Composite summary of models derived from Data Set 1 by various authors. ▨ Models falling inside a $\pm 0.04$ km/s, $\pm 0.2$ km band are centered on the correct model given in Fig. 1; — Other models; —— Tau-method bounds

synthetic section was also recalculated for the original model, using the same source function as for the other four cases, without adding numerical noise (A, Fig. 13).

The synthetic sections for models E, I and N are very similar and come closest to the original. A common difference from the original is a relatively weak $P_M P$ phase at distances greater than 110 km. In addition, phases from the middle crust are slightly more complicated in model I than in the original section between distances 40–90 km. The gradient in the upper crust of model N leads to greater amplitudes of the $P_g$ phase than observed originally. Additional phases originating from the low-velocity zones in models E and N cannot be resolved. The wave field for model L is characterized by higher amplitudes of all phases and a more rapid decrease with distance than in the original section.

All models presented in Fig. 3 are combined in one diagram in Fig. 14. For simplicity only models falling outside a $\pm 0.04$ km/s, $\pm 0.2$ km band centered on the correct model are displayed. The diagram also shows the Tau-method bounds derived by Bessonova, Fishman, Reznikov and Sitnikova which are not to be mistaken as possible velocity-depth models. As the stated deviation of allowed correlations by Bessonova et al. is rather small ($\pm 0.03$ s) it is not surprising that some of the other models fall outside the Tau-bounds in Fig. 14.

In conclusion it can be said that all models show the main boundaries at almost identical depths. This is due to the fact that all interpreters have identified the main phases in the same way. Differences in the models stem from small amplitude phases caused by numerical noise or interferences and by differences in the identification of phases which decay rapidly in amplitude with increasing distances. Although small variations in velocity, e.g. the

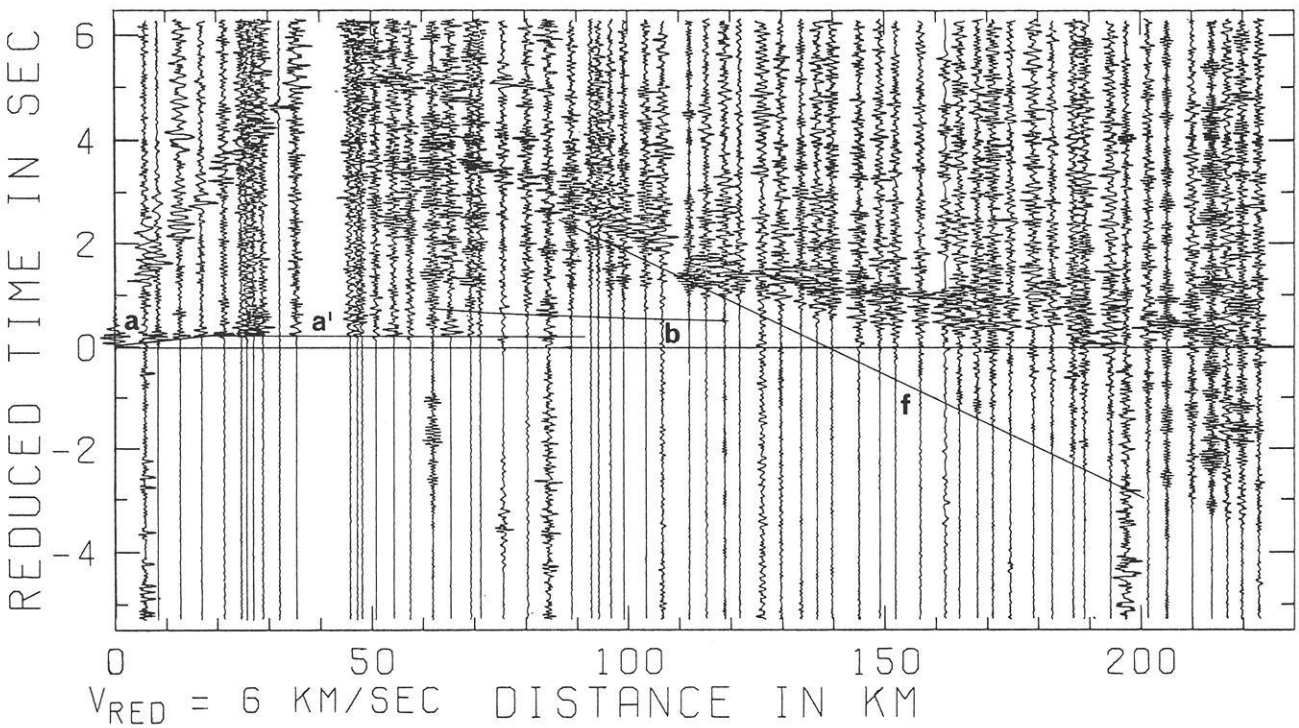


**Fig. 15.** Data Set 2: Distributed record section along profile LISPB ALPHA-1 (Bamford et al., 1976). The maximum peak to trough amplitude of each trace normalized to the same value before band-pass filtering 4–20 Hz. Correlation by Whitmarsh

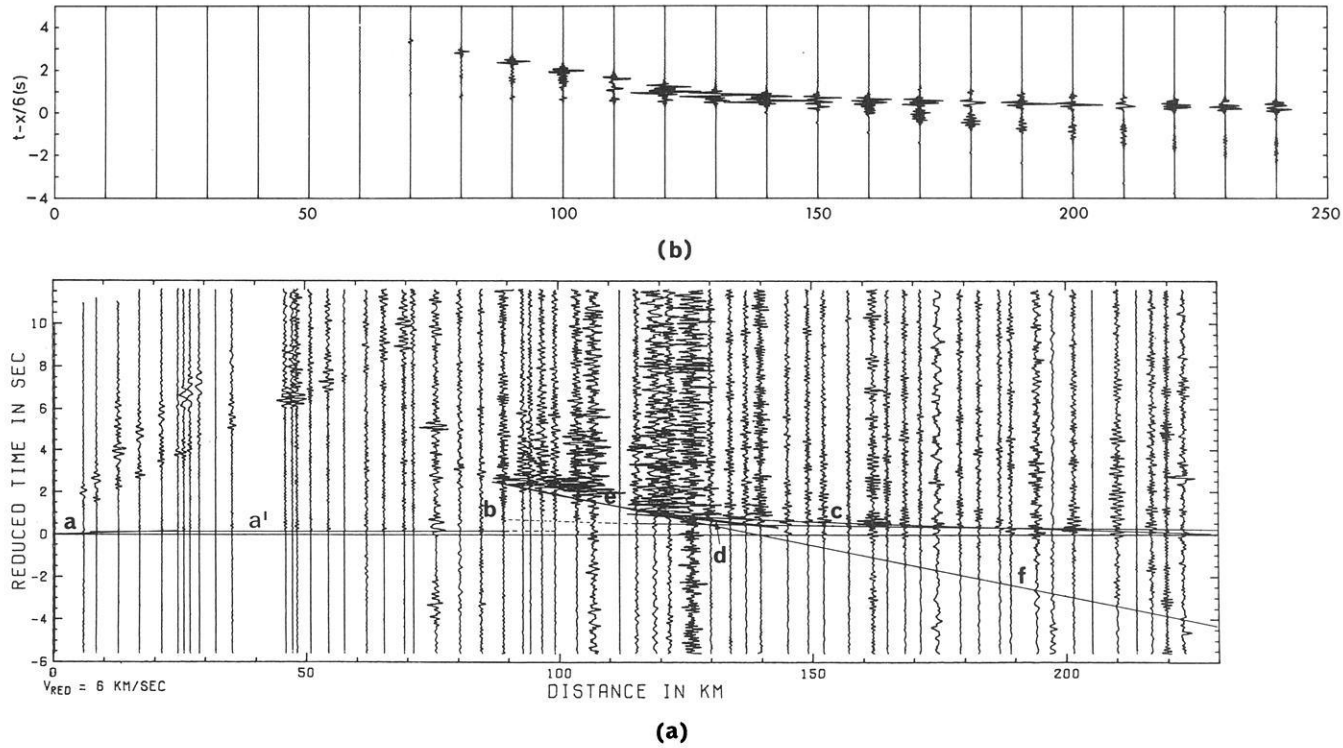


**Fig. 16. a** Observed record section along profile LISPB ALPHA-1 (Data Set 2). The traces were corrected to a common amplification factor, amplified by a factor proportional to distance squared and band-pass filtered 1–8 Hz. The hodochron branches are derived from the preferred velocity-depth model (Fig. 17). Lower case letters, also used in Fig. 17, denote the corresponding depth range from which each hodochron branch originates. **b** Synthetic record section calculated from the model in Fig. 17, assuming an infinite Q factor. Source was a delta function; integration between phase velocities of 6.0 and 10.0 km/s; band-pass filtering 1–8 Hz. Amplitudes proportional to distance squared (Whitmarsh)

deduced velocity reversals in models E, I and N, cannot be resolved, it is apparent from these examples that the use of synthetic seismograms during the interpretation of seismic refraction data is important in arriving at a model which approximates the truth from among the many possible velocity-depth models which satisfy the travel-time observations alone.

## Data Set 2: Crustal Record Section from the LISPB Experiment in Great Britain

The LISPB crustal record section (Fig. 15) was selected out of a series of crustal profiles recorded in 1974 in northern Britain (Bamford et al., 1976). This section was plotted with amplitudes normalized to the same maximum value in each trace and with broad-band filtering (1–30 Hz). During the workshop, the same data were replotted with the true amplitudes multiplied by distance squared (Fig. 16a) and with narrower band-pass filtering (e.g. 1–8 Hz). In the following some of the individual interpretations were selected with special emphasis on the personal approach of the author.

The interpretation by Whitmarsh (Figs. 15–17) is based mainly on arrivals identified on a true amplitude record section (Fig. 16a). The section shows two clear sets of arrivals which can be correlated from trace to trace. The first set is visible from 110 to 220 km and the arrivals have an apparent velocity of about 6.4 km/s. The second set is seen between 80 and 110 km, but can also be faintly discerned between 135 and 150 km, and contains arrivals with an apparent velocity of about 7.9 km/s. The above two

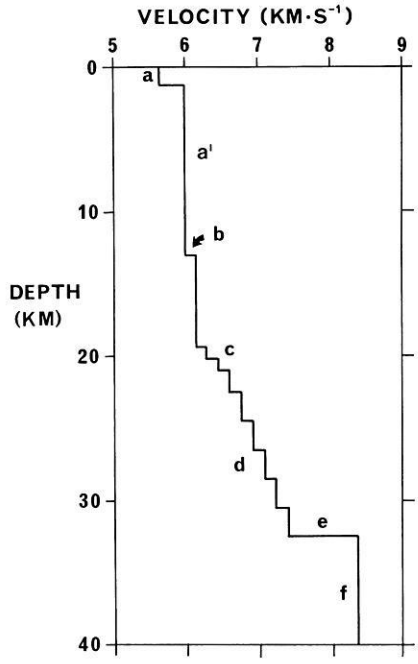


**Fig. 17.** Preferred velocity-depth model for Data Set 2 used to calculate the synthetic record section in Fig. 16b by Whitmarsh

phases are assigned to branches *c* and *e* respectively of a hodochron curve calculated from the final model (Figs. 16a and 17). The interpretation also depends to a lesser extent on the relatively high frequency normalized-amplitude record section (Fig. 15, originally distributed). This section

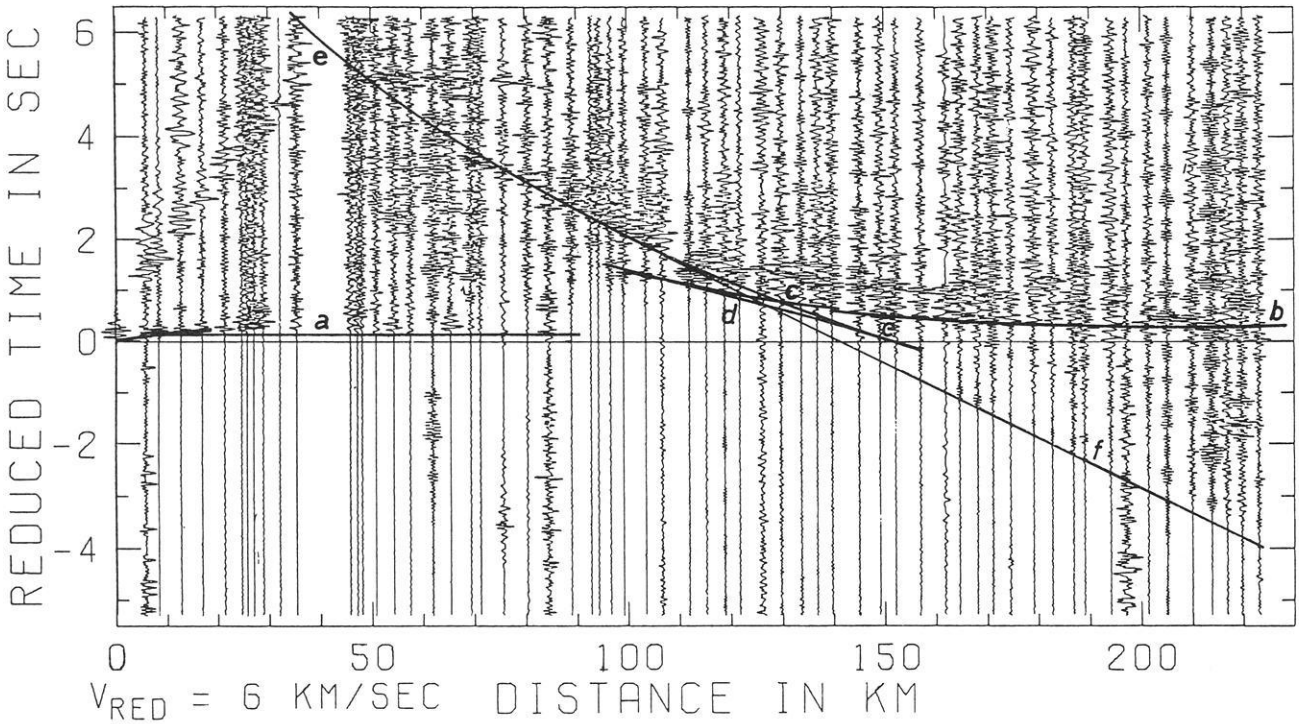


**Fig. 18.** Distributed LISPB ALPHA-1 section (Data Set 2) with travel-time curves according to the model in Fig. 19 by Mykkeltveit

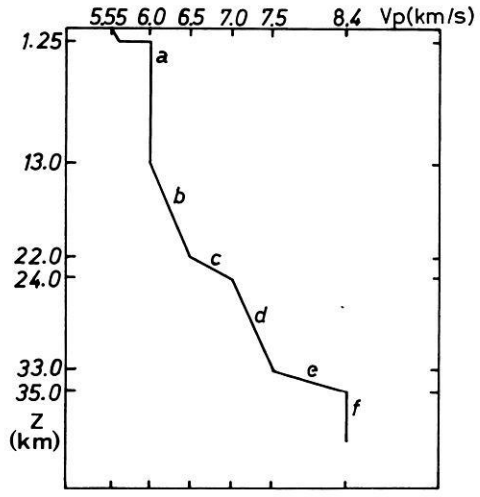


**Fig. 19.** Velocity-depth model derived by Mykkeltveit for Data Set 2

is valuable because it enables the identification of some other phases (falling on hodochron branches *a*, *a'* and *f*), which are too weak to be positively recognized on the true amplitude section (Fig. 16a). First arrivals at relatively short ranges, belonging to branches *a* and *a'*, are barely visible on Fig. 16a because of the distance-squared amplitude factor. A speculative branch *b* (Fig. 15) may also be identified, but the fact that the corresponding arrivals are apparently greatest in amplitude on traces where there is considerable noise before the first arrival means that some doubt exists as to the reality of this branch. It can also be poorly discerned on Fig. 16a. Lastly a branch *f* can be identified from a set of relatively high frequency first arrivals with an apparent velocity of about 8.4 km/s.

Various velocity-depth models were used to calculate hodochrons which fitted the observed times. Subsequently, synthetic seismograms were calculated for the most promising velocity-depth models by the reflectivity method (Fuchs and Müller, 1971), reaching a preferred model (Figs. 16b and 17). This model has a near constant velocity upper crust (6.0 km/s) and a lower crust of steadily increasing velocity (6.15–7.4 km/s) overlying a first-order Moho discontinuity at about 33 km depth.

According to Whitmarsh, the best models seem to be those for which the near cusps of the *b* and *c* retrograde branches occur beyond 110 km (so that only a relatively small amount of subcritically reflected energy appears at shorter ranges) while the *e–f* cusp occurs at about 90 km. Since arrivals of branch *d* are apparently not clearly seen, the positive gradient responsible for it was adjusted to give a very short prograde branch. Consequently, there are large phases at 130 and 140 km in Fig. 16b which are not evident in Fig. 16a. Although quite a satisfying fit of amplitudes has been obtained out to 160 km, the calculated amplitudes of supercritical reflections at greater ranges are systematically too great. An alternative conclusion is that the amplitudes at shorter ranges are too small, but it is hard to see how these amplitudes, particularly around the *e–f* cusp, could be radically increased. Since the calculated amplitude of wide-angle reflections at large distances is insensitive to changes in the velocity structure adjacent to the reflecting zone (Braile and Smith, 1975) the reason for the discrepancy may lie in the horizontal plane layered structure necessarily assumed for the synthetic seismogram program. In practice there may be significant lateral changes in structure causing the discrepancy, but these were not a subject of discussion.

Mykkeltveit (Figs. 18–20) interprets a variety of possible phase correlations in the distance range 90 to about 150 km. Several models yielding acceptable travel times have been

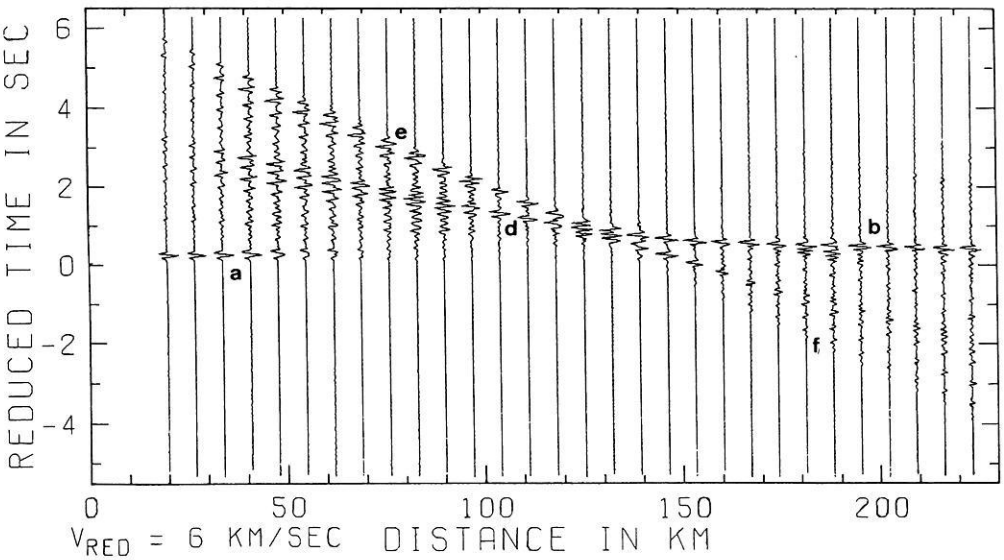


**Fig. 20.** Synthetic section calculated from the model in Fig. 19 by Mykkeltveit

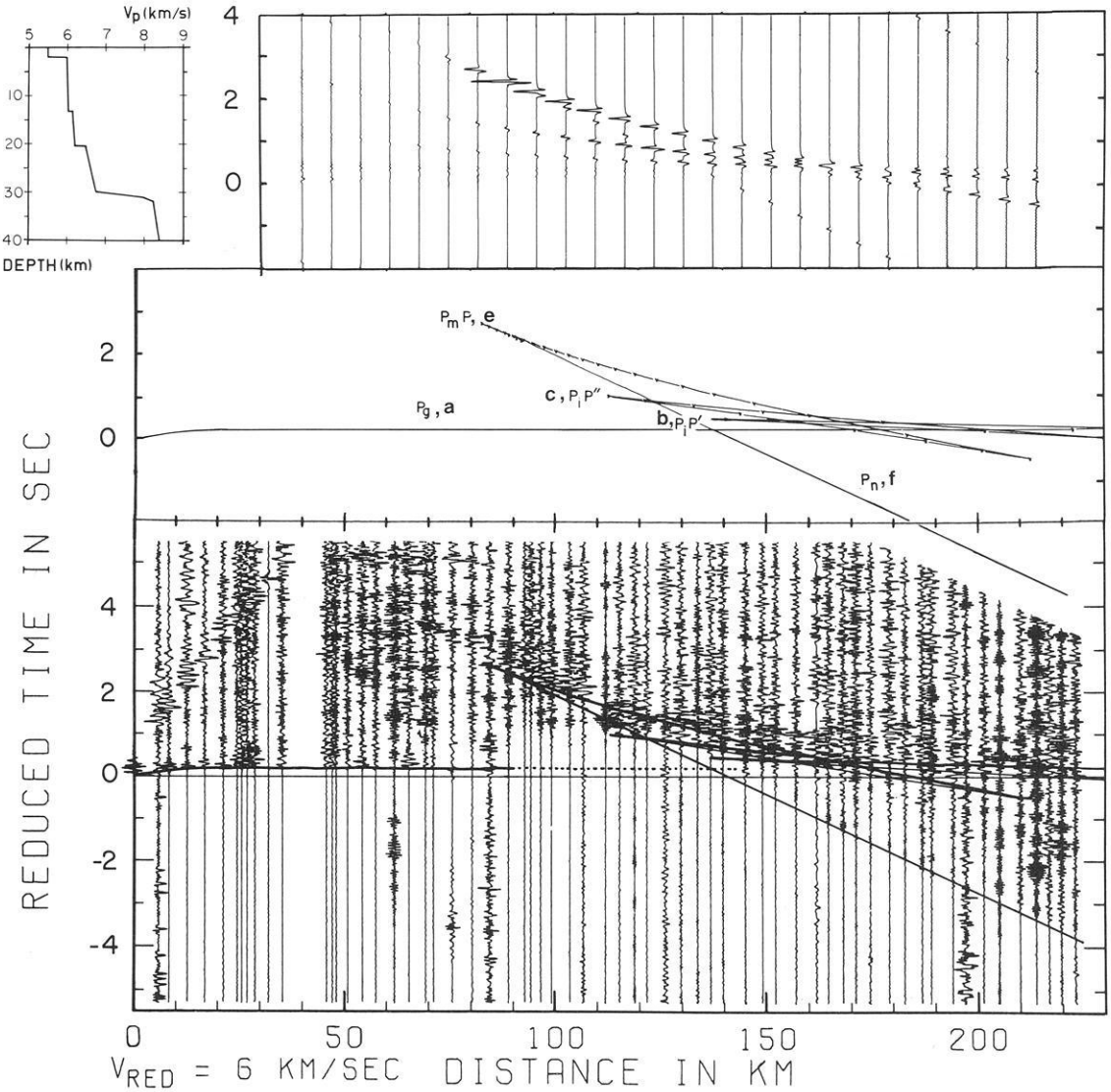


**Fig. 21.** An interpretation of Data Set 2 by Mooney; Original data with correlations, velocity-depth function, corresponding synthetic seismograms, and theoretical travel times.

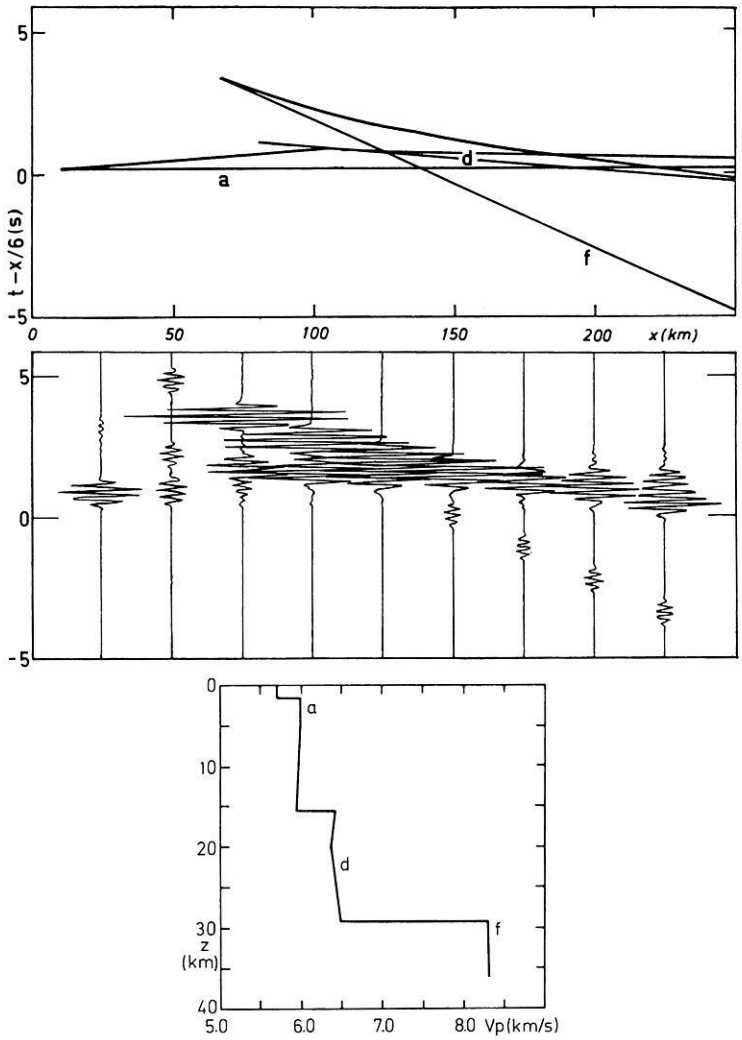


**Fig. 22.** Model, travel times and synthetic seismograms derived for Data Set 2 by Hill

derived all with identical structures above 13 km and below 35 km. These models were subsequently checked using normalized synthetic seismograms with the reflectivity method (after Fuchs and Müller, 1971). The model, shown in Fig. 19 with the resulting travel times shown on the record section of Fig. 18, has the following characteristics:

– The transition *b* provides – at least in part – an explanation for the large amplitudes observed at distances beyond about 150 km at a reduced arrival time of about 0.5 s.

– The layer *c* with a higher velocity gradient produces a reversal in the travel-time curve associated with relatively large amplitudes.

– A layer *d* with a gradient equal to the one of layer *b* results in a travel-time branch extending to less than 160 km. This feature, however, may not be satisfactorily modelled as can be seen from Fig. 20.

– The Moho, transition layer *e*, is associated with another reversal in the travel-time curve. The corresponding amplitudes on the synthetic section (Fig. 20) are slightly too high, but this and the overlying layer seem to be optimal in the sense that energy is being spread out in the triangular area between the branches *b* and *f* (Fig. 18). No correlation of phases can be made in this part of the section that could be attributed to a major first-order discontinuity of the velocity-depth curve.

In the interpretation of Mooney (Fig. 21) the direct wave ($P_g$) arrival is modelled with a 5.5 km/s surface velocity which rapidly reaches 6.0 km/s. A zero or very slightly positive upper crustal velocity gradient is assumed because of the low ($P_g/P_MP$) amplitude ratio at 70 km and beyond. A discontinuity at 13 km is indicated by the phase $P_iP'$ and a jump in seismic velocity from 6.05 km/s to 6.14 km/s was chosen to match the observed critical point and apparent velocity. Continuing in depth, the observed arrival times and apparent velocities of phases $P_iP''$ and $P_MP$ are modelled with discontinuities at 20 km and 31 km, respectively. The upper mantle velocity is based on the clear $P_n$ arrivals. Lateral heterogeneity is evidenced by the sudden 0.3 s offset in the $P_n$ arrival times between 195 km and 205 km. In this model (Fig. 21) the Moho discontinuity has been spread over a kilometer to avoid large amplitude subcritical reflections, and an initial mantle velocity of 8.0 km/s has been used to match the observed position of the $P_MP$ critical point. A positive velocity gradient below the Moho is indicated by the high $P_n$ apparent velocity and ($P_n/P_MP$) amplitude ratio.

Hill (Fig. 22) emphasizes a commonly observed aspect of crustal refraction profiles. In particular, the $P_g$ first arrivals appear to decay rather abruptly at distances of 60–80 km and the arrivals preceeding $P_n/P_MP$ between this distance

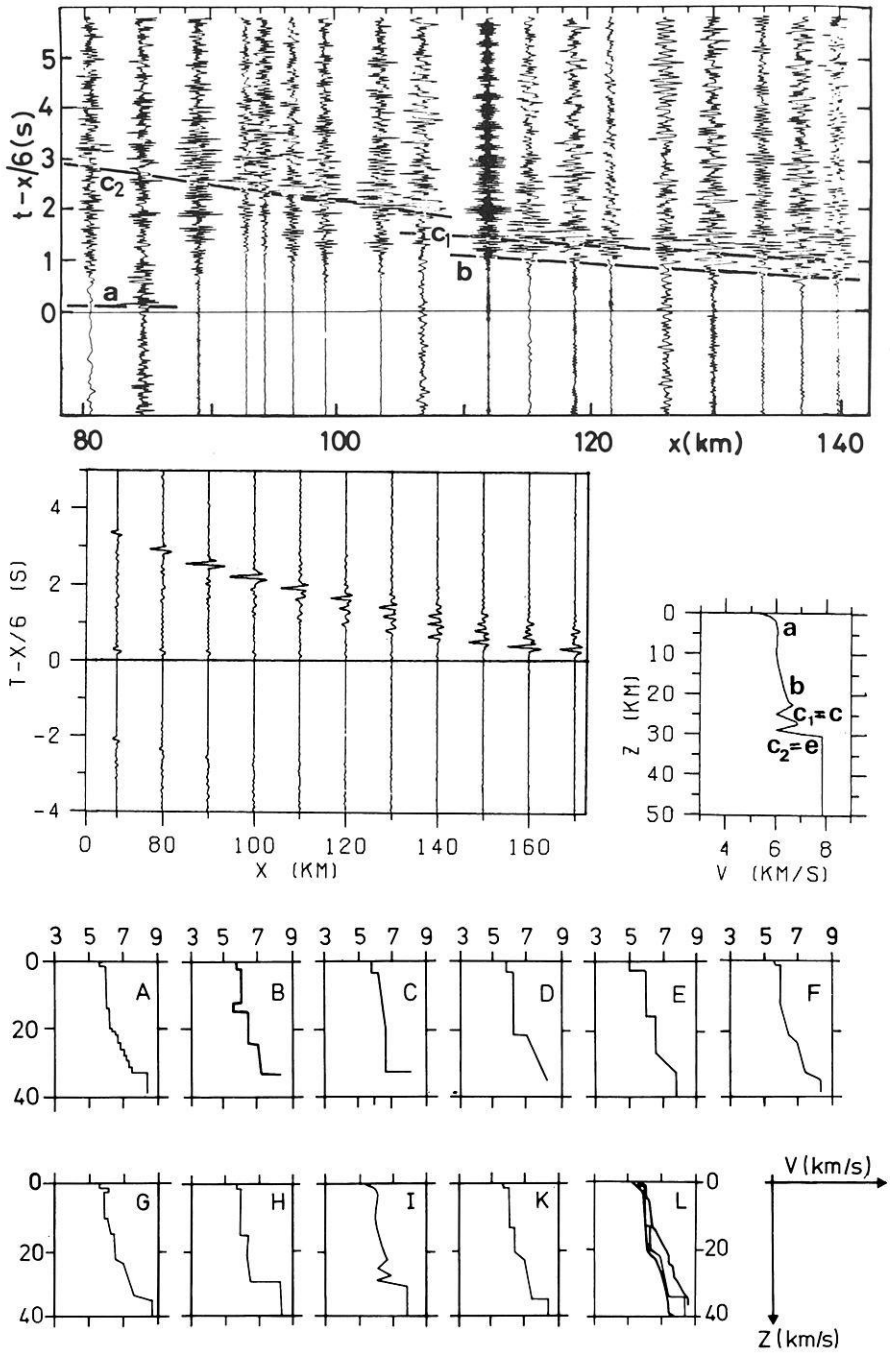


**Fig. 23.** Data Set 2 with correlations and velocity-depth function by Giese. The corresponding synthetic section was computed during the workshop




**Fig. 24.** Models derived from the real record section (Data Set 2) in Fig. 15 by various authors: *A*) Whitmarsh; *B*) Ansorge, Mueller, Banda; *C, D*) Kosminskaya; *E*) Braile; *F*) Mykkeltveit; *G*) Bamford et al., 1978; *H*) Hill; *I*) Giese; *K*) final model; *L*) Orcutt, Tau-bounds together with final model

range and the $P_n$ cross-over distance are often emergent with complicated wave patterns. One possible interpretation of this phenomenon is suggested in Fig. 22 involving slight negative velocity gradients beneath the major crustal refracting horizons. This model does seem to explain the features indicated, however, the intermediate phase is definitely too strong.

Giese (Fig. 23) correlates the later arrivals quite differently. While Whitmarsh, for example, correlates the wave $P_MP$ as a single group (Fig. 15), Giese tries a strict phase correlation (Fig. 23) thereby obtaining separate branches which are offset by 0.3–0.5 s. Applying the method described above, Giese derives a model which is characterized by a sequence of alternating high and low velocity zones in the lower crust (Fig. 23). The amplitude ratios in each trace of the synthetic section match the observations reasonably well.

Figure 24 shows a selection of velocity-depth functions derived for the LISPB crustal record section by various participants. The variety of these results reflects primarily the differences in phase correlations as was shown in detail by some examples. It can be concluded that in general all models show a clear crust-mantle boundary at about 35 km depth. Only two models show a slightly shallower Moho and in one model the Moho does not appear as a specific boundary. Velocity inversions are of minor importance. The transition to a higher-velocity lower crust has been located by most authors between 20 km and 25 km depth. While differences in details are quite obvious, the main characteristic properties, i.e. a more or less constant velocity in the

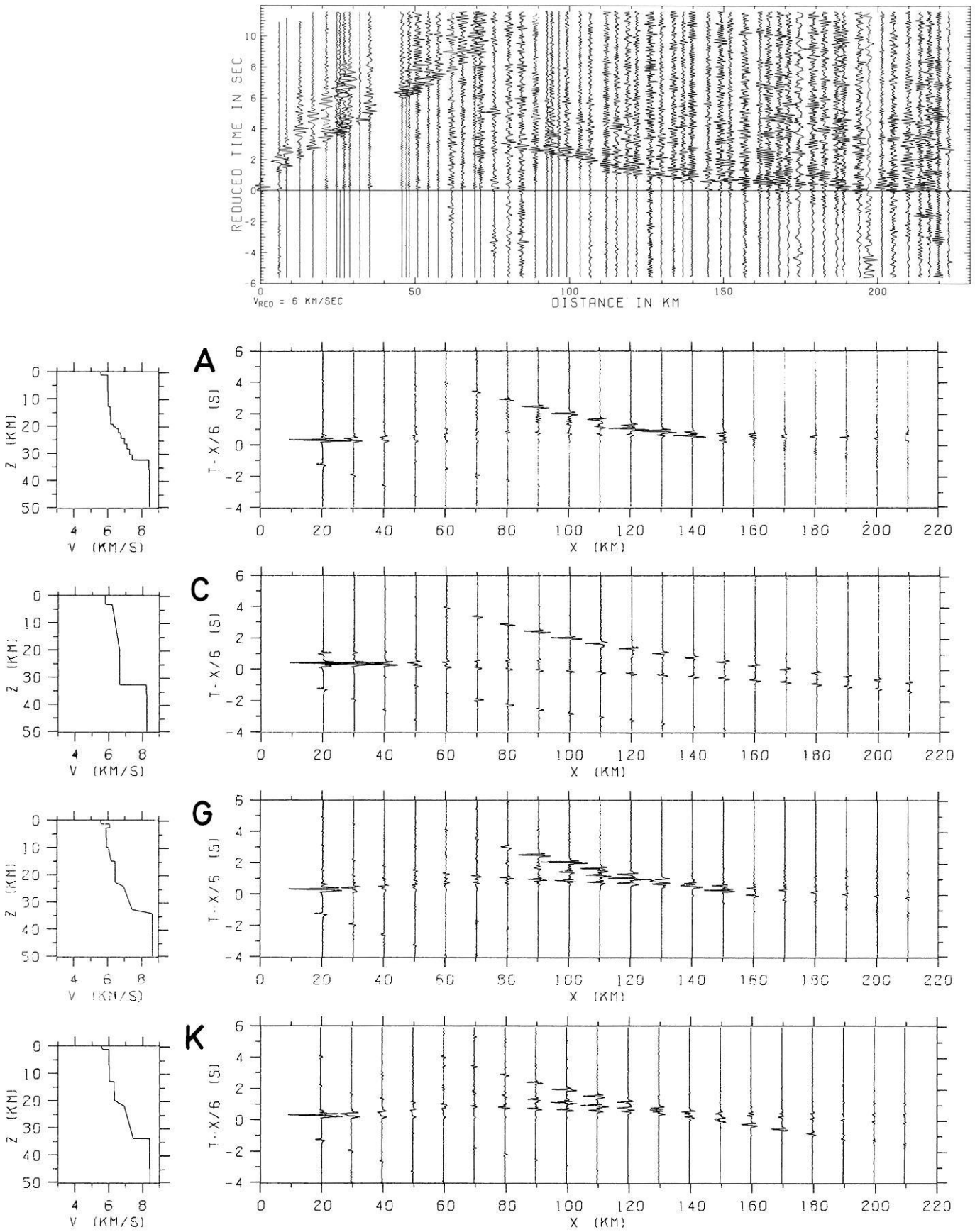


**Fig. 25.** Data Set 2 plotted with band-pass filter 1–8 Hz and normalized amplitudes together with synthetic sections calculated from various models (Fig. 24) including the final model (K) derived during the workshop

upper and a gradient zone in the lower crust, are rather well determined. During the workshop, after replotting the data with true amplitudes (Fig. 16a) and a narrower band-pass filtering (Fig. 25), the participants discussed extensively the possible correlations. This discussion resulted in the agreement that the velocity-depth function shown in Fig. 24 (Model K) may be the best one. Figure 24 also contains Tau-method bounds calculated by Orcutt for the same data (diagram L). Due to the independent correlations and error bounds this band of allowed velocities does not necessarily comprise all the models shown in this figure, though the final model (K) satisfies these conditions which were derived independently.

For some selected models synthetic seismogram sections were recalculated. They are presented in Fig. 25 together with a synthetic section for the agreed solution (model K in Fig. 24) and an original record section with a narrower band-pass filtering (1–8 Hz). The $P_g$ phase is best reproduced by models G and K. The velocity jump at about 15 km depth (models G, H, K) produces arrivals which can easily be recognized in the original section but with slightly too high amplitudes. Only an additional strong velocity increase between 20 and 25 km depth connected with a positive velocity gradient in the lower crust provides the observed energy recorded in front of the large amplitude phases at 80–100 km and beyond 150 km distance (models G and K). The large amplitude phases between 80 and 150 km are basically fitted by all models. However, the critical distance for the $P_MP$ phase resulting from model H is slightly too short because of the large velocity contrast at the crust-mantle boundary and its shallower depth. In addition to the data presented here, the reversed and overlapping record sections together with a geological section were available during the workshop (Bamford et al., 1978). These illustrated quite clearly the need to take full account of lateral variations when interpreting explosion seismic data. In the present case a laterally homogeneous structure had to be assumed for the interpretation of the selected data.

## Conclusions

A comparison of the final results (Figs. 3, 14, and 24) for the synthetic data set and for the observed record section may be a good starting point for a concluding discussion. The models for the synthetic record section scatter much less in their velocity-depth distribution than those for the real data set. These differences are quite obvious from the much narrower range of possible correlations in data set 1 as compared to the large variability in data set 2. The variety of velocity-depth functions computed for these data prior to the workshop reflects primarily the differences in the correlation of phases of the various workers. The different methods of inversion applied subsequently lead to structures with the same main features when the initial correlations are similar. The inversion technique has only a minor influence on the character of the model. To some extent preconceived ideas about the velocity structure on the part of the individual interpreter may bias the number and identification of correlations. This results in structural details which can only be verified with high quality data and amplitude modelling.

Apart from clearly correlatable refracted arrivals (i.e. $P_g$ and $P_n$ phases) the most reliable waves for estimating the main parameters of the velocity model are the reflections, especially if they are recorded at undercritical distances. They enable the determination of depths of boundaries and the corresponding average velocities with very high accuracy. For this purpose all methods are good enough, even approximate formulas for homogeneous media, if the results are controlled by direct travel-time calculations. The correlation of short and weak phases is problematic and can be the reason for major differences in derived structure.

The scatter of models for the LISPB data could be reduced considerably during the workshop by the use of a true amplitude record section with appropriate filtering. The final model (Fig. 24) satisfies the data best if lateral variations are neglected. The participants of the workshop realized, however, that better criteria are needed for a more objective and reliable correlation of phases. As a basic result it can be stated that the main effort has to be put into the acquisition of dense and high quality data which then have to be subjected to a careful processing with filtering and true amplitude recoverage as a basis for any inversion method. In addition, inversion methods for inhomogeneous media should be further developed and applied. The interpretation of seismic data obtained in inhomogeneous media was one of the topics of the subsequent workshop by the Commission on Controlled Source Seismology at Park City, Utah (USA), in 1980 (Mooney, 1981). The same subject will be further discussed at the next meeting in Zürich in 1983.

*Acknowledgments.* The participants would like to express their gratude to the staff of the Geophysical Institute in Karlsruhe for the successful organization of the workshop. The support of some of the participants by the German Research Society (Deutsche Forschungsgemeinschaft) is greatly acknowledged. The Computer Center of the University of Karlsruhe, the Geophysical Institute, and the Faculty of Physics provided immediate and ample access to their computing and other facilities. We gratefully acknowledge the improvement of the manuscript by K. Fuchs and the helpful comments of one of the reviewers. We thank E. Hirzel for typing the manuscript.

## References

Bamford, D., Faber, S., Jacob, B., Kaminski, W., Nunn, K., Prodehl, C., Fuchs, K., King, R., Willmore, P.: A lithospheric seismic profile in Britain – I. Preliminary results. Geophys. J. R. Astron. Soc. **44**, 145–160, 1976

Bamford, D., Nunn, K., Prodehl, C., Jacob, B.: LISPB-IV Crustal structure of Northern Britain. Geophys. J.R. Astron. Soc. **54**, 43–60, 1978

Bamford, D., Kosminskaja, I., Mueller, S., Prodehl, C.: The results of the C.C.S.S. Workshop at Karlsruhe. Tectonophysics **56**, 126, 1979

Bessonova, E.N., Fishman, V.M., Ryaboyi, V.Z., Sitnikova, G.A.: The tau method for inversion of travel times – I. Deep seismic sounding data. Geophys. J. R. Astron. Soc. **36**, 377–398, 1974

Bessonova, E.N., Fishman, V.M., Shnirman, M.G., Sitnikova, G.A., Johnson, L.R.: The tau method for inversion of travel times – II. Earthquake data. Geophys. J. R. Astron. Soc. **46**, 87–108, 1976

Braile, L.W., Smith, R.B.: Guide to the interpretation of crustal refraction profiles. Geophys. J.R. Astron. Soc. **40**, 145–176, 1975

Červený, V., Molotkov, I.A., Pšenčík, I. Ray method in seismology. Praha. Univerzita Karlova 1977

Fuchs, K., Müller, G.: Computation of synthetic seismograms with the reflectivity method and comparison with observations. Geophys. J. R. Astron. Soc. **23**, 417–433, 1971

Gerver, M.L., Markushevich, V.M.: Determination of the seismic wave velocity from their travel-time curves. Calculation seismology, 3. Moscow: Nauka 1967

Geyko, V.S.: Determination of the velocity peculiarity for the gradient medium and kinematic features of the refractions from their travel-time curves. Geophysical Sbornik, 33. Kiev: Naukova Dumka 1970

Giese, P.: Depth calculation. In: Explosion Seismology in Central Europe, P. Giese, C. Prodehl, A. Stein, eds.: pp. 146–161. Berlin, Heidelberg, New York: Springer 1976

Jurov, J.G.: Crust cross section of the Russian Platform. In: Seismic models of the main geostructures in the USSR. Moscow: Nauka 1978

Mykkeltveit, S.: A seismic profile in southern Norway. Pageoph. **118**, 1310–1325, 1980

Mooney, W.D.: IASPEI Workshop: Seismic modelling of laterally varying structures. EOS **61**, 19, 1981

Pavlenkova, N.I., Smeljanskaja, T.V.: Methods of the velocity determination from the refraction travel-time curves. Geophysical Sbornik, 29. Kiev: Naukova Dumka 1969

Riznichenko, J.V.: Geometrical seismic of the layered medium. Trudu ITG, AN SSSR, Moscow, 1946

Received March 4, 1982; Revised version June 28, 1982
Accepted July 2, 1982